The Astrophysical Journal, 653:361–382, 2006 December 10

THE GLOBAL EVOLUTION OF GIANT MOLECULAR CLOUDS. I. MODEL FORMULATION AND QUASI-EQUILIBRIUM BEHAVIOR

Mark R. Krumholz[1]
Department of Astrophysical Sciences, Princeton University, Princeton, NJ 08544-1001; krumholz@astro.princeton.edu

Christopher D. Matzner
Department of Astronomy, University of Toronto, Toronto, ON M5S 3H8, Canada; matzner@cita.utoronto.ca

and

Christopher F. McKee
Departments of Physics and Astronomy, University of California, Berkeley, CA 94720-7304; cmckee@astron.berkeley.edu
Received 2006 May 1; accepted 2006 August 11

ABSTRACT

We present semianalytic dynamical models for giant molecular clouds evolving under the influence of H II regions launched by newborn star clusters. In contrast to previous work, we neither assume that clouds are in virial or energetic equilibrium, nor do we ignore the effects of star formation feedback. The clouds, which we treat as spherical, can expand and contract homologously. Photoionization drives mass ejection; the recoil of cloud material both stirs turbulent motions and leads to an effective confining pressure. The balance between these effects and the decay of turbulent motions through isothermal shocks determines clouds' dynamical and energetic evolution. We find that for realistic values of the rates of turbulent dissipation, photoevaporation, and energy injection by H II regions, the massive clouds where most molecular gas in the Galaxy resides live for a few crossing times, in good agreement with recent observational estimates that large clouds in Local Group galaxies survive roughly 20–30 Myr. During this time clouds remain close to equilibrium, with virial parameters of 1–3 and column densities near 10^{22} H atoms cm^{-2}, also in agreement with observed cloud properties. Over their lives they convert 5%–10% of their mass into stars, after which point most clouds are destroyed when a large H II region unbinds them. In contrast, small clouds like those found in the solar neighborhood only survive $\sim$1 crossing time before being destroyed.

Subject headings: H II regions — ISM: clouds — stars: formation

1. INTRODUCTION

Giant molecular clouds (GMCs) are the primary reservoirs of molecular gas within spiral galaxies. Star formation is tightly correlated with the molecular column density within spiral galaxies (Wong & Blitz 2002), and is therefore controlled by the formation and evolution of these giant clouds. In this and a subsequent paper we develop the theory of GMC dynamics and present semianalytical models for GMC evolution. We rely on simplifying assumptions about the structure of the cloud and the properties of the surrounding interstellar medium in order to focus on clouds' global energy budget and dynamical state.

Observations show that stars form much more slowly than the free-fall rate in GMCs (Zuckerman & Evans 1974; Rownd & Young 1999; Wong & Blitz 2002; Gao & Solomon 2004; Wu et al. 2005), and any successful GMC model must explain why this should be. It is now widely held that collapse is inhibited primarily by intensely supersonic motions (Vázquez-Semadeni et al. 2003; Mac Low & Klessen 2004), rather than magnetic fields (Mouschovias & Spitzer 1976; Shu et al. 1987; McKee 1989). (Star formation is strongly suppressed in low-extinction regions of molecular clouds, beyond what one would expect if the star formation rate were simply following the column density to some power, suggesting that magnetic fields may play a secondary role [Onishi et al. 1998, 1999, 2002; Johnstone et al. 2004], although see Hatchell et al. [2005], who find that low column densities reduce but do not completely prevent star formation.) Simulations and analytic theory indicate that the observed level of turbulence in GMCs is sufficient to produce the observed rate of star formation (Krumholz & McKee 2005).

However, undriven supersonic turbulence decays via radiation from isothermal shocks with an *e*-folding time of roughly 1 cloud crossing time (Mac Low et al. 1998; Stone et al. 1998; Mac Low 1999; Padoan & Nordlund 1999), so undriven turbulence alone is not sufficient to prevent global collapse. Instead, either GMCs must be destroyed before their turbulent motions decay, or the turbulence must be continually driven. The mode of destruction is intimately related to the clouds' dynamical state. Unless a cloud is destroyed all at once, any internal agent of destruction is also an internal source for turbulent energy—and one strong enough to balance turbulent decay (Matzner 2002). Destruction from within therefore favors models that achieve energetic and dynamical equilibrium (e.g., McKee 1989), if only briefly. The alternative—that clouds are disrupted entirely by outside agents (e.g., Bonnell et al. 2006)—requires most of the cloud mass to remain gravitationally unbound, as bound regions rapidly collapse to higher density and become impervious to external forces. This is very difficult to reconcile with observational estimates of GMCs' lifetimes and ratios of kinetic to potential energy. We critique the hypothesis of unbound clouds in greater detail in § 7.

In the following sections, we investigate the properties of molecular clouds both stirred and destroyed by H II regions within the cloud volume. The models we present here are improved in several ways relative to prior work:

1. Rather than enforcing strict mechanical or energetic equilibrium, we solve for the time evolution of a cloud's radius and turbulent velocity dispersion according to the time-dependent virial and energy equations. In an early discussion of this problem, McKee (1989) allowed for time dependence in the energy equation, but assumed virial equilibrium. Matzner (1999) and Matzner & McKee (1999) followed the evolution of GMCs

[1] Hubble Fellow.

using time-dependent virial and energy equations, but neglected several terms in these equations that we model here. While our approach is still not a full numerical solution of the equations of gravity, radiation, and magnetohydrodynamics, this approach enables us to study cloud dynamics without ignoring the effects of feedback on GMC evolution, as most numerical simulations to date have done (e.g., Clark et al. 2005).

2. We account self-consistently for the recoil of cloud matter from the sites of mass ejection. In addition to driving turbulence, inward recoil confines the cloud. Recoil confinement is equivalent to an additional (and variable) external pressure, which becomes dynamically significant when cloud destruction is rapid. Corresponding terms appear in the virial (§ 2.1; Appendix A) and energy (§ 2.2; Appendix B) equations.

3. Our model for H II regions (§ 3.2) accounts for the scale dependence of density and velocity structures within GMCs. Although this does not fully account for the three-dimensional structure of the turbulent cloud medium, it is a significant improvement over the uniform cloud model employed by Whitworth (1979) Williams & McKee (1997) and Matzner (2002).

4. We apply the Krumholz & McKee (2005) prescription for the star formation rate within turbulent clouds. This formula accurately predicts the star formation rate on a variety of scales, from starburst galaxies to the dense precursors of individual star clusters (Tan et al. 2006; Krumholz & Tan 2006). We use it to govern the birth rate of ionizing associations (§ 4).

5. Our dynamical simulations (§ 5) track the formation and evolution of many individual H II regions. This approach accounts for the finite lifetime of ionizing stars and the time delay associated with the deceleration of shells driven by H II regions, neither of which is negligible compared to GMC dynamical times.

We analyze the results of our models in § 6, discuss the implications of our findings in § 7, and summarize our conclusions in § 8. In a future work (C. D. Matzner, M. R. Krumholz, & C. F. McKee 2006, in preparation, hereafter Paper II) we apply this model to the problem of GMC formation and evolution in the galactic environment, including the effects of spiral density waves.

We do make several approximations in our work (§ 7.4). We assume that the clouds are spherical and that they expand or contract homologously. We assume that the clouds are sufficiently massive that the energy injection is dominated by H II regions, not protostellar outflows, which based on the models of Matzner (2002) should be true for clouds of mass $\sim 10^5\,M_\odot$ or more. Such clouds contain most of the molecular mass in the Galaxy. We neglect the possibility that the column density of the cloud must exceed a threshold in order for stars to form (e.g., McKee 1989). We neglect energy injection by H II regions after they reach pressure equilibrium with the surrounding medium. Finally, we neglect possible time-dependent effects due to the ambient medium of the GMC: no mass can be added to the cloud, and the ambient pressure remains constant. Despite these approximations, the models we present in this paper illustrate the degree to which GMC properties can be understood in terms of internal dynamics.

Obviously, real GMCs are not homologously expanding or contracting spheres with smooth density distributions, so the approximations we make to render the problem analytically tractable are quite limiting. For this reason one might be tempted give up on analytic treatment altogether and simply attempt to solve the problem numerically. Unfortunately, full numerical simulation of a GMC, including the formation of multiple star clusters and the effects of their feedback, is not feasible with current codes and computers. Instead, one is forced to make numerous approximations regardless of whether one takes a numerical or analytic approach. Many numerical simulations of GMC evolution simply ignore feedback altogether (e.g., Clark et al. 2005), include it only from a single source and/or focus on size scales much smaller than an entire GMC (e.g., Dale et al. 2005; Li & Nakamura 2006), or focus on the galactic scale and lack the resolution to say anything about individual GMCs (e.g., Slyz et al. 2005; Tasker & Bryan 2006). For this reason, an analytic approach that allows us to include feedback provides a valuable complement to numerical results, and points out areas for future simulation in which new effects might be discovered by a more thorough treatment of the physics.

2. EVOLUTION EQUATIONS

We are interested in the global evolution and energy balance in GMCs, so we construct a simple model in which we neglect details of cloud structure. We consider a cloud with density profile $\rho = \rho_e (r/R_{\rm cl})^{-k_\rho}$, where $R_{\rm cl}$ is the radius of the cloud edge and ρ_e is the edge density. As we discuss below, we take $k_\rho = 1$ as typical of GMCs. We approximate that the cloud evolves homologously, so that k_ρ is constant. However, the cloud can expand or contract and can lose mass (via evaporation of gas by H II regions), so ρ_e and $R_{\rm cl}$ both vary in time. The cloud is embedded in an ambient medium of negligible density and constant pressure $P_{\rm amb}$. We model evaporation of gas from the cloud as a wind, into which cloud material is injected at a rate $\dot{\rho}$ (which we take to be negative). Gas that is injected into the wind travels radially outward with "kick" velocity $\boldsymbol{v}'_{\rm ej}$ relative to the radial velocity of the cloud at that radius. Homology requires that the mass-loss rate follow the existing density profile, so

$$\dot{\rho} = \frac{\dot{M}_{\rm cl}}{M_{\rm cl}}\rho, \tag{1}$$

where $M_{\rm cl}$ is the total mass of the cloud. We assume that the wind is low density and escapes from the vicinity of the cloud quickly, so that we can neglect its gravitational interaction with the cloud. As we discuss in more detail in § 3.2, this is a reasonable model for mass evaporating from an H II region.

We neglect the possibility that turbulent motions within the cloud are likely to lead to a significant loss of mass. This seems justified, since in a GMC with a virial ratio of unity, roughly the value for observed GMCs, the 3D turbulent velocity dispersion is smaller than the escape speed from the GMC surface by a factor of ~ 2. Since the distribution of velocities in a supersonically turbulent medium cuts off exponentially above the turbulent velocity dispersion (Krumholz et al. 2006a), there is a negligible amount of mass moving rapidly enough to escape. We also neglect the possibility that a GMC might gain mass during its evolution, due to continuing infall. This assertion is more problematic, and we discuss it in more detail in § 7.4.

Within the limitations of these assumptions, we derive the Eulerian virial theorem (EVT) and equation of energy conservation in Appendices A and B. We then use these to construct evolution equations for the cloud.

2.1. *Equation of Motion*

We derive the equation of motion from the EVT for an evaporating homologously moving cloud,

$$\frac{1}{2}\ddot{I}_{\rm cl} = 2(\mathcal{T} - \mathcal{T}_0) + \mathcal{B} + \mathcal{W} - \frac{1}{2}\frac{d}{dt}\int_{S_{\rm vir}} (\rho \boldsymbol{v} r^2)\cdot d\boldsymbol{S} + 2a_I \dot{M}_{\rm cl} R_{\rm cl}\dot{R}_{\rm cl} + \frac{1}{2}a_I \ddot{M}_{\rm cl} R_{\rm cl}^2 + \frac{3-k_\rho}{4-k_\rho}\dot{M}_{\rm cl} R_{\rm cl} v'_{\rm ej}. \tag{2}$$

The proof of this theorem is in Appendix A. In this equation $I_{\rm cl}$ is the cloud moment of inertia, $\mathcal{T}$ is the total kinetic and thermal energy, $\mathcal{T}_0$ is the energy associated with the confining external pressure, $\mathcal{B}$ and $\mathcal{W}$ are the magnetic and gravitational potential energies, and the surface integral represents the rate of change of the flux of inertia across the surface $S_{\rm vir}$ that bounds the volume to which we apply the virial theorem. These are all terms that appear in the EVT for a cloud without a wind, and their formal definitions are given in Appendix A. The three additional terms represent the second derivative of cloud inertia caused by mass loss through the wind (the first two extra terms) and the rate at which recoil from the process of launching the wind injects momentum into the cloud (the final additional term).

We now evaluate each of these terms in the context of our model. The moment of inertia is $I_{\rm cl} = a_I M_{\rm cl} R_{\rm cl}^2$, where $a_I \equiv (3 - k_\rho)/(5 - k_\rho)$, so its second derivative is

$$\frac{1}{2}\ddot{I}_{\rm cl} = a_I M_{\rm cl}\dot{R}_{\rm cl}^2 + a_I M_{\rm cl} R_{\rm cl}\ddot{R}_{\rm cl} + 2a_I \dot{M}_{\rm cl} R_{\rm cl}\dot{R}_{\rm cl} + \frac{1}{2}a_I \ddot{M}_{\rm cl} R_{\rm cl}^2. \tag{3}$$

Next consider the kinetic term $\mathcal{T}$, which we evaluate by decomposing the velocity into large-scale homologous and fluctuating turbulent components (eq. [A8]). This gives

$$\mathcal{T} = \frac{3}{2}M_{\rm cl}c_{\rm cl}^2 + \frac{1}{2}a_I M_{\rm cl}\dot{R}_{\rm cl}^2 + \mathcal{T}_{\rm turb} + 2\pi P_{\rm amb}(R_{\rm vir}^3 - R_{\rm cl}^3), \tag{4}$$

where $c_{\rm cl}$ is the sound speed in the cloud (assumed constant), $\mathcal{T}_{\rm turb}$ is the term for turbulent motions, and the last term comes from the constant ambient pressure $P_{\rm amb}$ outside the cloud. We return to $\mathcal{T}_{\rm turb}$ below. Note that our assumption of homologous motion implicitly neglects the possibility of significant rotational motions. Observed GMCs have negligible kinetic energies in overall rotation compared to turbulent motions or gravitational potential energy.

We use the same strategy for the gravitational and magnetic terms as for the kinetic term, dividing them into steady and fluctuating parts. The nonturbulent gravitational part is

$$\mathcal{W}_{\rm non\text{-}turb} = -\frac{3}{5}a\frac{GM_{\rm cl}^2}{R_{\rm cl}}, \tag{5}$$

where

$$a = \frac{15 - 5k_\rho}{15 - 6k_\rho}. \tag{6}$$

In principle we should include a component of potential energy due to stars, but all observed molecular clouds have gas masses that greatly exceed their stellar masses. For this reason, we can neglect the stellar mass. For the nonturbulent magnetic component, we follow McKee et al. (1993). Let Φ be the total magnetic flux threading the cloud, so that the mean field within the cloud is $\bar{B} = \Phi/(\pi R_{\rm cl}^2)$. From the form of the magnetic energy term (eq. [A13]), it is clear that the nonturbulent component of this term scales as $\mathcal{B}_{\rm non\text{-}turb} \propto \bar{B}^2 R_{\rm cl}^3$. We therefore define the constant b such that

$$\mathcal{B}_{\rm non\text{-}turb} = \frac{b}{3}\bar{B}^2 R_{\rm cl}^3 = \frac{b}{3\pi^2}\left(\frac{\Phi^2}{R_{\rm cl}}\right). \tag{7}$$

The exact value of b depends on the topology of the magnetic field and on the background field B_0, but it is generally of order unity, with $b = 0.3$ as a typical value (McKee et al. 1993). We now define the magnetic critical mass M_Φ by

$$M_\Phi^2 = \left(\frac{5b}{9\pi^2 a}\right)\frac{\Phi^2}{G}, \tag{8}$$

so that we have

$$\mathcal{B}_{\rm non\text{-}turb} = \frac{3}{5}a\frac{GM_\Phi^2}{R_{\rm cl}}. \tag{9}$$

We define the magnetic support parameter by

$$\eta_B = \frac{M_\Phi}{M_{\rm cl}}. \tag{10}$$

With this definition, we can combine the nonturbulent magnetic and gravitational terms to find

$$\mathcal{W}_{\rm non\text{-}turb} + \mathcal{B}_{\rm non\text{-}turb} = -\frac{3}{5}a(1 - \eta_B^2)\frac{GM_{\rm cl}^2}{R_{\rm cl}}. \tag{11}$$

Now consider the turbulent components. First, we can neglect the turbulent component of the gravitational term since most subregions of a molecular cloud are not self-gravitating (Krumholz & McKee 2005), and therefore have negligible potential energy in comparison to their kinetic or magnetic energies. We can therefore set $\mathcal{W} = \mathcal{W}_{\rm non\text{-}turb}$. For the magnetic and kinetic turbulent components, McKee & Zweibel (1992) argue for equipartition of kinetic and magnetic energy. Stone et al. (1998) find in simulations of low plasma-β turbulence that magnetic energy is slightly subequipartition, $\mathcal{B}_{\rm turb} \approx 0.6\mathcal{T}_{\rm turb}$, which McKee & Tan (2003) argue can be understood as the kinetic and magnetic energies reaching equipartition for motions transverse to the field, but not for motions along the field. We adopt the ratio of magnetic to kinetic energy found by Stone et al. (1998), so the combined turbulent kinetic and magnetic energies in the virial theorem are

$$2\mathcal{T}_{\rm turb} + \mathcal{B}_{\rm turb} \approx 2.6\mathcal{T}_{\rm turb} = 3.9M_{\rm cl}\sigma_{\rm cl}^2, \tag{12}$$

where $\sigma_{\rm cl} = \langle (v_z - v_{{\rm cl},z})^2 \rangle_\rho^{1/2}$ is the one-dimensional mass-weighted turbulent velocity dispersion of the gas in the cloud.

Finally, we come to the surface terms, $\mathcal{T}_0$ and $(d/dt)\int_{S_{\rm vir}} (\rho \boldsymbol{v}\boldsymbol{r}^2)\cdot d\boldsymbol{S}$. We can make the latter term zero by choosing our virial surface to be well outside the cloud so that the density of cloud material on the surface is negligible. However, the pressure outside the cloud $P_{\rm amb}$ is nonzero, so

$$\mathcal{T}_0 = 2\pi P_{\rm amb} R_{\rm vir}^3. \tag{13}$$

Substituting into the EVT (eq. [2]), we arrive at an equation of motion for the cloud:

$$a_I\ddot{R}_{\rm cl} = 3.9\frac{\sigma_{\rm cl}^2}{R_{\rm cl}} + 3\frac{c_{\rm cl}^2}{R_{\rm cl}} - \frac{3}{5}(1 - \eta_B^2)a\frac{GM_{\rm cl}}{R_{\rm cl}^2} - 4\pi P_{\rm amb}\frac{R_{\rm cl}^2}{M_{\rm cl}} + \left(\frac{3 - k_\rho}{4 - k_\rho}\right)\frac{\dot{M}_{\rm cl}}{M_{\rm cl}}v_{\rm ej}'. \tag{14}$$

This equation is intuitively easy to understand. The left-hand side represents the acceleration of the cloud edge, which is equated with the force per unit mass due to internal turbulence and pressure (the first two terms), gravity and magnetic fields (the third term), external pressure (the fourth term), and recoil from the evaporating gas (the final term).

For convenience we wish to nondimensionalize this equation. Let $M_{\rm cl,0}$, $R_{\rm cl,0}$, and $\sigma_{\rm cl,0}$ be the initial mass, radius, and velocity dispersion of the cloud. We define the dimensionless variables $M = M_{\rm cl}/M_{\rm cl,0}$, $R = R_{\rm cl}/R_{\rm cl,0}$, $\sigma = \sigma_{\rm cl}/\sigma_{\rm cl,0}$, and $\tau = t/t_{\rm cr,0}$, where $t_{\rm cr,0} = R_{\rm cl,0}/\sigma_{\rm cl,0}$ is the crossing time of the initial cloud. In these variables equation (14) becomes

$$R'' = \frac{3.9\sigma^2 + 3\mathcal{M}_0^{-2}}{a_I R} - \eta_G \frac{M}{R^2} - \eta_P \frac{R^2}{M} + \eta_R \frac{M'}{M}, \quad (15)$$

where the primes indicate differentiation with respect to τ,

$$\eta_G \equiv \frac{3a(1-\eta_B^2)}{a_I \alpha_{\rm vir,0}}, \quad (16)$$

$$\eta_P \equiv \frac{4\pi R_{\rm cl,0}^3 P_{\rm amb}}{a_I M_{\rm cl,0}\sigma_{\rm cl,0}^2}, \quad (17)$$

$$\eta_R \equiv \left(\frac{3-k_\rho}{4-k_\rho}\right)\frac{v'_{\rm ej}}{a_I \sigma_{\rm cl,0}}, \quad (18)$$

and we have defined the initial Mach number

$$\mathcal{M}_0 \equiv \frac{\sigma_{\rm cl,0}}{c_{\rm cl}} \quad (19)$$

and nonthermal virial parameter (Bertoldi & McKee 1992)

$$\alpha_{\rm vir,0} \equiv \frac{5\sigma_{\rm cl,0}^2 R_{\rm cl,0}}{GM_{\rm cl,0}}. \quad (20)$$

If the cloud's initial state is in equilibrium and it is not losing mass, so $R'(0) = M'(0) = 0$, then the ambient pressure $P_{\rm amb}$ must be such that

$$\eta_P = \frac{3.9 + 3\mathcal{M}_0^{-2}}{a_I} - \eta_G. \quad (21)$$

Note that this generally implies an ambient pressure higher than the mean in the ISM. We consider it realistic, however, because GMCs form in relatively overpressured regions, and because we have not included the weight of an atomic layer overlying the cloud. Once mass loss commences, there will be an additional recoil pressure.

2.2. *Equation of Energy Evolution*

To derive the evolution equation for the cloud energy, we begin with the general energy conservation equation for an evaporating homologous cloud, which we derive in Appendix B and for convenience repeat here:

$$\frac{d\mathcal{E}}{dt} = \frac{\dot{M}_{\rm cl}}{M_{\rm cl}}\left[\mathcal{E} + (1-\eta_B^2)\mathcal{W}\right] - 4\pi P_{\rm amb} R_{\rm cl}^2 \dot{R}_{\rm cl} + \left(\frac{3-k_\rho}{4-k_\rho}\right)\dot{M}_{\rm cl}\dot{R}_{\rm cl} v'_{\rm ej} + \mathcal{G}_{\rm cl} - \mathcal{L}_{\rm cl}. \quad (22)$$

Here $\mathcal{E}$ is the total cloud energy, and $\mathcal{G}_{\rm cl}$ and $\mathcal{L}_{\rm cl}$ are the rates of radiative energy gain and loss integrated over the entire cloud. This equation is easy to understand intuitively. The term $(\dot{M}_{\rm cl}/M_{\rm cl})\mathcal{E}$ is simply the mass-loss rate times the energy per unit mass in the cloud. The term $(\dot{M}_{\rm cl}/M_{\rm cl})(1-\eta_B^2)\mathcal{W}$ is the rate at which mass loss reduces the cloud energy via reduction of the gravitational and magnetic fields, both of which are proportional to the mass. The next two terms represent the rate at which the external pressure and the recoil force from launching the wind do work on the cloud. Finally, the last two terms are simply the rate of radiative gains and losses.

Using the same arguments as in § 2.1, we can write the total energy in the cloud as

$$\mathcal{E} = \frac{1}{2}a_I M_{\rm cl}\dot{R}_{\rm cl}^2 + 2.4 M_{\rm cl}\sigma_{\rm cl}^2 + \frac{3}{2}M_{\rm cl}c_{\rm cl}^2 - \frac{3}{5}a(1-\eta_B^2)\frac{GM_{\rm cl}^2}{R_{\rm cl}}. \quad (23)$$

Note that the factor of 2.4 in the $M_{\rm cl}\sigma_{\rm cl}^2$ term comes from taking $\mathcal{T}_{\rm turb} + \mathcal{B}_{\rm turb} \approx 1.6\mathcal{T}_{\rm turb}$, and the 3/2 in front of the $M_{\rm cl}c_{\rm cl}^2$ term comes from the assumption that the ratio of specific heats for the cloud is $\gamma_{\rm cl} = 5/3$. One might expect 7/5 instead, since the cloud is molecular and therefore diatomic. However, the lowest rotational or vibrational excitations of H_2 have excitation temperatures of several hundred K. Since the cloud is far colder than this, molecules never have enough energy to access their rotational and vibrational degrees of freedom, and the gas acts as if it were monatomic. The time derivative of this is

$$\frac{d\mathcal{E}}{dt} = \frac{1}{2}a_I\dot{M}_{\rm cl}\dot{R}_{\rm cl}^2 + a_I M_{\rm cl}\dot{R}_{\rm cl}\ddot{R}_{\rm cl} + 2.4\dot{M}_{\rm cl}\sigma_{\rm cl}^2 + 4.8 M_{\rm cl}\sigma_{\rm cl}\dot{\sigma}_{\rm cl} + \frac{3}{2}\dot{M}_{\rm cl}c_{\rm cl}^2 - \frac{6}{5}a(1-\eta_B^2)\frac{GM_{\rm cl}\dot{M}_{\rm cl}}{R_{\rm cl}} + \frac{3}{5}a(1-\eta_B^2)\frac{GM_{\rm cl}^2\dot{R}_{\rm cl}}{R_{\rm cl}^2}. \quad (24)$$

Substituting $\mathcal{E}$ and $d\mathcal{E}/dt$ into the energy equation (22), we find

$$a_I M_{\rm cl}\dot{R}_{\rm cl}\ddot{R}_{\rm cl} + 4.8 M_{\rm cl}\sigma_{\rm cl}\dot{\sigma}_{\rm cl} + \frac{3}{5}a(1-\eta_B^2)\frac{GM_{\rm cl}^2}{R_{\rm cl}^2}\dot{R}_{\rm cl} = -4\pi P_{\rm amb}R_{\rm cl}^2\dot{R}_{\rm cl} + \left(\frac{3-k_\rho}{4-k_\rho}\right)\dot{M}_{\rm cl}\dot{R}_{\rm cl}v'_{\rm ej} + \mathcal{G}_{\rm cl} - \mathcal{L}_{\rm cl}. \quad (25)$$

We may regard this as an evolution equation for $\sigma_{\rm cl}$, which makes intuitive sense: the overall expansion and contraction of the cloud is dictated by the equation of motion, and the thermal energy per unit mass is fixed, so the turbulence acts as the energy reservoir, increasing or decreasing as the cloud gains or loses energy. Rearranging to solve for $\dot{\sigma}_{\rm cl}$ and nondimensionalizing as we have done with the equation of motion gives

$$\frac{4.8}{a_I}\sigma' = -\frac{R'R''}{\sigma} - \eta_G\frac{MR'}{R^2\sigma} - \eta_P\frac{R^2R'}{M\sigma} + \eta_R\frac{M'R'}{M\sigma} + \frac{\mathcal{G}-\mathcal{L}}{a_I M\sigma}, \quad (26)$$

where $\mathcal{G}$ and $\mathcal{L}$ are the dimensionless rates of radiative energy gain and loss, defined by

$$\mathcal{G} - \mathcal{L} = \left(\frac{R_{\rm cl,0}}{M_{\rm cl,0}\sigma_{\rm cl,0}^3}\right)(\mathcal{G}_{\rm cl} - \mathcal{L}_{\rm cl}). \quad (27)$$

3. ENERGY SOURCES AND SINKS

In this section we evaluate the rates of radiative energy gain $\mathcal{G}$ and loss $\mathcal{L}$, and the characteristic launch speed of evaporating gas $v'_{\rm ej}$. Together with the equation of motion (15) and the energy equation (26), and the star formation rate (§ 4), this will completely specify the evolution of our model clouds.

3.1. *Decay of Turbulence via Isothermal Shocks*

GMCs are approximately isothermal because their radiative timescales are much shorter than their mechanical timescales. As a result, supersonic motions within the cloud generate radiative shocks that remove energy from the cloud. The problem of the decay of turbulent motions by supersonic isothermal shocks in both hydrodynamic and magnetohydrodynamic media has been studied extensively by numerical simulation (e.g., Mac Low et al. 1998; Stone et al. 1998; Mac Low 1999; Padoan & Nordlund 1999). Stone et al. (1998) find that the dissipation timescale of the turbulent energy is $t_{\rm dis} \equiv \dot{E}/E = 0.83\lambda_{\rm in}/v_{\rm rms} = 0.48\lambda_{\rm in}/\sigma$, where $\lambda_{\rm in}$ is the length scale on which the energy is injected.

In reality, H II regions coming from associations of various sizes, winds, and gravitational contraction of the cloud will all contribute to turbulent motions and inject energy on different length scales. However, we can estimate an effective length scale through a combination of observational and theoretical considerations. Observationally, turbulence in nearby GMCs appears to be driven on scales comparable to the cloud scale or larger (Basu & Murali 2001; Heyer & Brunt 2004), and theoretical estimates of the effective energy injection scale of H II regions suggest that this is also near the cloud scale (Matzner 2002). The longest wavelength mode that a cloud of radius $R_{\rm cl}$ can support is $\sim 4R_{\rm cl}$, where the factor of 4 arises because the largest turbulent mode corresponds to overall expansion or contraction of the cloud, in which diametrically opposed points are moving in opposite directions. Motion in opposite directions corresponds to the points being half a wavelength apart, giving a total wavelength of twice the cloud diameter (Matzner 2002). Thus, we take the effective injection scale to be $\lambda_{\rm in} = 4\phi_{\rm in}R_{\rm cl}$, where $\phi_{\rm in} \leq 1$, and we take $\phi_{\rm in} = 1$ as a fiducial value based on observations and theory. The (dimensionless) rate at which energy is radiated away due to decaying turbulence is

$$\mathcal{L} = \frac{\eta_v}{\phi_{\rm in}} \frac{M\sigma^3}{R}, \tag{28}$$

where the simulations of Stone et al. give $\eta_v = 1.2$. Note that in deriving this factor, we have used our result that the energy in the turbulence, including magnetic and kinetic contributions, is $2.4M_{\rm cl}\sigma_{\rm cl}^2$.

It is also worth noting the possibility that the measured energy loss rates are too high. Cho & Lazarian (2003) argue that Alfvén waves cascade and decay anisotropically, and that this anisotropy can reduce the decay rate. However, Cho & Lazarian argue that simulations to date have not captured this effect because they use an isotropic driving field that is unrealistic. Sugimoto et al. (2004) simulate filamentary molecular clouds, and find that Alfvén waves of certain polarizations decay more slowly than simulations have found. Even if neither of these effects apply, there are differences in the rate of decay in different simulations depending on how the turbulence is driven. The simulations of Mac Low (1999) give slightly lower dissipation rates, probably because in those simulations the turbulence is forced with a driving field that is constant in time, while in those of Stone et al. (1998) the driving field is determined randomly at each time step. While we feel that the Stone et al. approach is somewhat more realistic, this is by no means certain.

3.2. H II *Regions*

H II regions are the dominant source of energy injection into GMCs from within (Matzner 2002). We consider the effects of the H II region from a single association here, and extend our results to a population of associations in § 4.

3.2.1. *Evolution of Individual* H II *Regions*

We first describe the evolution of an H II region embedded in a molecular cloud, modifying the analysis by Matzner (2002) by allowing the mean ambient density and velocity dispersion to vary with radius r away from the formation site of an association, as $\rho(r) \propto r^{-k_\rho}$ and $\sigma(r) \propto r^{-k_\sigma}$, respectively. Matzner (2002) considered only the homogeneous case $k_\rho = k_\sigma = 0$. Note that the local turbulent virial parameter $\alpha(r) \equiv 5r\sigma^2(r)/[GM(r)]$ scales as $r^{k_\rho - 2k_\sigma - 2}$. Since $\alpha(r)$ is roughly unity on the scale of the cloud and on that of the newborn association (else it would not have formed), it is reasonable to assume $k_\rho = 2k_\sigma + 2$. The observed line width–size relation and density-size relations (Solomon et al. 1987) imply $k_\sigma = -1/2$ and $k_\rho = 1$, and we adopt these values below. These parameters correspond to a cloud with a negligible internal pressure gradient. Note that it has been suggested that the observational result $k_\rho = 1$ (which is equivalent to GMCs having constant column densities within a galaxy) is simply an observational artifact (e.g., Vazquez-Semadeni et al. 1997). However, many of the proposed mechanisms to explain how this artifact could be created do not apply to extragalactic observations, and more recent observations show that GMCs in other galaxies also show constant column densities (Blitz et al. 2006 and references therein). We discuss this point in more detail in §§ 6.2 and 7.3, and also refer readers to the discussion of this point in Krumholz & McKee (2005).

The density variation affects the expansion phase of the H II region, and the variation in velocity dispersion affects how H II regions merge with the background turbulence. The evolution of an H II region in a turbulent GMC is a substantial problem that must ultimately be solved via simulation. However, to date only preliminary attempts to solve the problem have been made (e.g., Dale et al. 2005; Mellema et al. 2006; Mac Low et al. 2006; Krumholz et al. 2006b), so we are forced to rely an analytic approximations.

First, consider the expansion phase of an H II region. Assume that it has expanded well beyond its initial Strömgen radius. The mean ambient density is $\bar{\rho}(r) \propto r^{-k_\rho}$ within a distance r from the association, the ionized gas temperature is $T_{\rm II} \simeq 7000$ K, the (constant) ionizing luminosity is $S = 10^{49}S_{49}$ s^{-1}, and the recombination coefficient is $\alpha^{(2)}$ in the on-the-spot approximation. If the H II region is blister-type, ionized gas will rocket away from the ionization front at a velocity $v'_{\rm ej} = 2c_{\rm II}$, where $c_{\rm II} = 9.74$ km s^{-1} is the sound speed in the ionized gas. This is the characteristic launch velocity of our cloud's escaping wind. For the evolution of the H II region, Matzner's dynamical equation (his eq. [15]) admits the self-similar solution

$$r_{\rm sh}^2 \bar{\rho}(r_{\rm sh}) = (2,\ 1) \times \frac{3}{4} \frac{(7-2k_\rho)^2}{9-2k_\rho} \rho_{\rm II} c_{\rm II}^2 t^2 \tag{29}$$

for (blister, embedded) regions. Here $r_{\rm sh}$ is the radius of the shell at time t, and $\rho_{\rm II}$ is the (uniform) density inside the H II region, which must vary as $r_{\rm sh}^{-3/2}$ to ensure that ionizations balance recombinations. This equation applies when the expansion velocity is much larger than the turbulent velocity dispersion; we discuss the effects of turbulence below. This yields

$$r_{\rm sh}^{7/2} \bar{\rho}(r_{\rm sh}) = (2,\ 1) \times 2.2 \frac{3(7-2k_\rho)^2}{2(9-2k_\rho)} k_{\rm B} T_{\rm II} \left(\frac{3S}{4\pi\alpha^{(2)}}\right)^{1/2} t^2, \tag{30}$$

where $k_{\rm B}$ is Boltzmann's constant. The leading factor of 2.2 accounts for the particle abundances assuming helium is singly

and the main sequence ionizing lifetime is

$$\langle t_{\rm ms} \rangle_a = \frac{\langle s_{49}(m) t_{\rm ms}(m) \rangle_{\rm IMF}}{\langle s_{49}(m) \rangle_{\rm IMF}}, \quad (46)$$

where $s_{49}(m)$ and $t_{\rm ms}(m)$ are the ionizing luminosity (in units of 10^{49} photons s^{-1}) and main-sequence lifetime of a star of mass m. We adopt the fits of Parravano et al. (2003) for $s(m)$ and $t_{\rm ms}(m)$, which, together with the Kroupa (2001) IMF, give $\langle s_{49}(m) \rangle_{\rm IMF} = 7.2 \times 10^{-4}$, $S_{49} = 3.4 \times 10^{-3} (M_a/M_\odot)$, and $t_{\rm ms} = 3.8$ Myr. However, for smaller associations the ionizing luminosity is likely to be dominated by the single most massive star, and this causes the ionizing luminosity function to flatten and the ionizing lifetime to vary with s_{49}. McKee & Williams (1997, Appendix A) give an analytic formula that approximates the flattening, but for semianalytic models we can dispense with the approximation and determine the luminosity function simply by drawing stars randomly from the IMF until we accumulate mass up to a given association mass. We can then determine the ionizing luminosity of the association by summing those of the individual stars, and define the main-sequence lifetime as the time at which the stars providing half the ionizing photons disappear.

Note that in contrast to Williams & McKee (1997) and Matzner (2002), we do not impose an absolute upper limit of $S_{49} \leq 490$ on the ionizing luminosity of associations. This has no effect at all on any but the most massive clouds, since the requirement that the association mass be at most 10% of the cloud mass imposes a limit on S_{49} that is lower than this. For the most massive clouds we model in § 6.1, the largest associations formed reach $S_{49} \sim 1700$, but the extremely weak dependence of H II region properties on S_{49} ($r_{\rm sh} \propto S_{49}^{1/5}$) means that increasing the maximum S_{49} by a factor of a few has very little effect. Furthermore, due to the relative improbability of forming an association so close to the upper mass limit, even for our highest mass models the majority of clouds do not form associations with $S_{49} > 490$. Thus, we do not expect the presence or absence of an upper limit on association ionizing luminosities to affect our results in any significant way.

5. SEMIANALYTIC MODELS

5.1. *Methodology*

We now have in place all the necessary theoretical apparatus to set up our semianalytic models. In essence, our model describes the evolution of a GMC using a pair of coupled nonlinear ODEs (ordinary differential equations), with added damping and driving terms. We integrate these equations forward in time in a three-step process. First, we use the current configuration of the cloud to compute the rate of turbulent decay (eq. [28]), the rate of star formation (eq. [40]), and the rate of evaporation by H II regions (eq. [33]). We update $R_{\rm cl}$, $\dot{R}_{\rm cl}$, $\sigma_{\rm cl}$, and $M_{\rm cl}$ using these values (eqs. [15] and [26]). We chose our update time step so that no quantity changes by more than 0.1% per advance. Second, we update the state of H II regions as described in § 3.2. We compute new values of the radius and expansion rate for each H II region, removing those whose expansion rates are low enough or radii are large enough for them to merge. At merging, we add their energy to turbulent motions in the cloud.

Third, we create new H II regions. To do this we generate a random mass for the next association, chosen from the distribution given in equation (44). We track the amount of mass transformed into stars since the last association was fully formed, and when half the next association mass has been accumulated in new stars, we add an H II region for that association. To determine the properties of the H II region, we generate stellar masses from the Kroupa (2001) IMF, assign an ionizing luminosity and main-sequence lifetime to each star, and use these to compute the total ionizing luminosity and lifetime (defined as the time when the stars responsible for half the ionizing photons burn out) for the association. We continue to put newly formed stars into the new association until the full mass of the association has been accumulated, at which point we reset the tally of accumulated stellar mass and randomly generate a new mass for the next association.

We terminate the evolution when one of three conditions has been satisfied: (1) an H II region unbinds the cloud [i.e., $r_{\rm sh} \geq R$ and $\dot{r}_{\rm sh} > (2GM/R)^{1/2}$]; (2) the cloud surface density has dropped to the point where its visual extinction $A_V < 1.4$, the minimum required for CO to remain molecular (van Dishoeck & Black 1988), assuming the standard Milky Way interstellar UV field and dust-to-gas ratio, whereby 1 g cm^{-2} corresponds to $A_V = 214$; or (3) the time step is less than 10^{-8} times the current evolution time, which occurs if the radius is approaching zero. We term these possibilities *disruption*, *dissociation*, and *collapse*. An important caveat that applies to all these outcomes is their dependence on our assumption of spherical symmetry. Even if an H II region delivers an impulse capable of unbinding a cloud, the cloud may actually be displaced as a whole, or it may break into multiple pieces, each of which is internally bound and capable of continuing to form stars. In the case of dissociation, a GMC's mean column density may be so low that much of its mass is turned atomic by the interstellar UV field, but overdense clumps within it may survive and continue star formation. Finally, the collapse case would probably result in a cloud fragmenting into smaller pieces rather than undergoing monolithic collapse, as occurs in our one-dimensional models.

TABLE 1
FIDUCIAL PARAMETERS

Parameter	Value
$\alpha_{\rm vir,0}$	1.1
c_s	0.19 km s^{-1}
η_B	0.5
η_E	1.0
η_v	1.2
k_ρ	1.0
$\phi_{\rm in}$	1.0

5.2. *Fiducial Initial Conditions*

Here we describe a basic set of initial conditions for our runs. In § 6 we discuss how varying some of these affects the outcome of our runs. Our models start with a common set of initial parameters summarized in Table 1. Most of these values are taken directly from observations, but a few of the parameters deserve some additional discussion. Observations of the strength of magnetic fields in GMCs are quite uncertain. We set $\eta_B = 0.5$, corresponding to equipartition between magnetic and kinetic energy. For a more detailed analysis of the observational data and theoretical arguments for this choice, see Krumholz & McKee (2005, § 7.3). We set $\eta_v = 1.2$ and $\phi_{\rm in} = 1.0$, corresponding to the decay of turbulence at the rate found by the simulations of Stone et al. (1998) and to turbulence on the size scale of the entire GMC. Finally, we set $\eta_E = 1$, corresponding to H II regions injecting energy into turbulent media as efficiently as they would for smooth media.

With these parameters fixed, we can fully specify the initial conditions for a model by giving the initial mass and column density of a cloud. We evolve models with masses of $M_{\rm cl,6} = 0.2$, 1.0, and 5.0, where $M_{\rm cl} = M_{\rm cl,6} \times 10^6\ M_\odot$. These masses

TABLE 2
Initial Cloud Properties

$M_{\rm cl,6}$	$N_{\rm H,22}$	$R_{\rm cl,0}$ (pc)	$\sigma_{\rm cl,0}$ (km s^{-1})	$t_{\rm cr,0}$ (Myr)
0.2.....	0.5	33.7	2.37	13.9
1.0.....	0.5	75.3	3.54	20.8
5.0.....	0.5	168	5.30	31.1
0.2.....	1.5	19.4	3.12	6.1
1.0.....	1.5	43.5	4.66	9.1
5.0.....	1.5	97.2	6.97	13.6
0.2.....	4.5	11.2	4.10	2.7
1.0.....	4.5	25.1	6.14	4.0
5.0.....	4.5	56.1	9.18	6.0

span the range where most of the molecular gas in the Milky Way resides (Williams & McKee 1997). We set the initial cloud column density to $N_{\rm H,22} = 1.5$, where $N_{\rm H} = N_{\rm H,22} \times 10^{22}$ cm^{-2}, which is typical for Milky Way GMCs regardless of mass (Larson 1981; Solomon et al. 1987). We summarize the initial radius, velocity dispersion, and crossing time as a function of mass in Table 2. For reference, we also show how these quantities vary with column density at fixed mass.

6. RESULTS

6.1. *Fiducial Runs*

We simulate the fiducial initial conditions 100 times each, using different random seeds for each run, for each of our three initial masses. Table 3 summarizes the statistical outcome of our fiducial runs.

The most basic result is that massive clouds attain a quasi-equilibrium state, in which the decay of turbulence is roughly balanced by the injection of energy by H II regions. In this state, cloud virial parameters fluctuate around unity, but most clouds spend most of their lives with virial parameters from 1 to 3, with a time-averaged value from 1.5 to 2.2 depending on the cloud mass, as shown by Figure 1. This may slightly overestimate the true virial parameter, because in our model we assume that all of the energy from H II regions goes into random turbulent motions that can then fuel cloud expansion, rather than into coherent motions of the cloud as a whole or, if H II regions fragment the cloud, into motions of these fragments. Such coherent motions are often excluded in observational estimates of virial parameters. Nonetheless, at a qualitative level the result that clouds equilibrate to virial parameters $\sim$1 is in good agreement with observations showing that massive clouds are approximately virialized (Heyer et al. 2001; Blitz et al. 2006).

The evolution follows a sawtooth pattern, in which an H II region drives up the virial parameter, which then exponentially

TABLE 3
Fiducial Run Outcomes

$M_{\rm cl,6}$ (1)	$t_{\rm life}$ (2)	$\bar{\alpha}_{\rm vir}$ (3)	$\bar{N}_{\rm H,22}$ (4)	SFE (5)	$M_{\rm phot}$ (6)	$N_{\rm disrupt}$ (7)	$N_{\rm dissoc}$ (8)	$N_{\rm col}$ (9)
0.2.....	1.6 (9.9)	2.2	1.4	0.053	0.59	63	37	0
1.0.....	2.2 (20)	2.1	1.3	0.054	0.70	92	8	0
5.0.....	3.2 (43)	1.5	1.5	0.082	0.80	99	1	0

Notes.—Col. (2): Mean lifetime in crossing times (parentheses give corresponding value in Myr). Cols. (3)–(4): $\alpha_{\rm vir}$ and $N_{\rm H,22}$ averaged over all times and runs. Col. (5): Star formation efficiency. Col. (6): Fraction of mass photoevaporated prior to cloud destruction. Cols. (7)–(9): Number of runs out of 100 that ended in disruption, dissociation, and collapse.

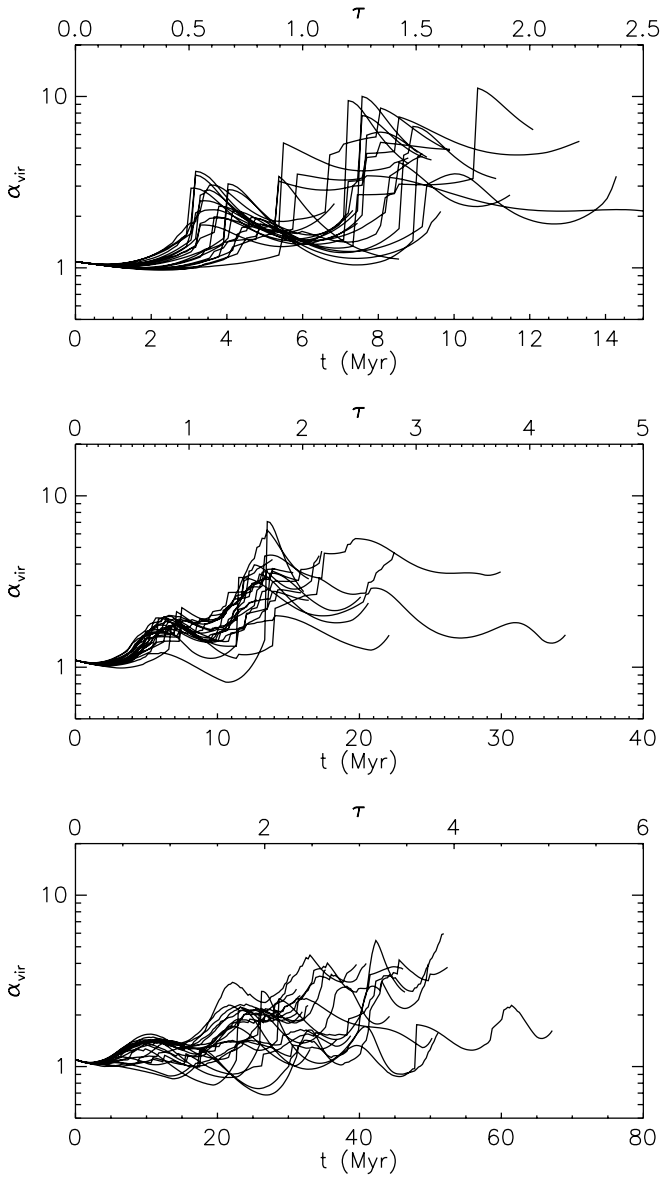

Fig. 1.—Virial parameter $\alpha_{\rm vir}$ vs. physical time t and dimensionless time τ for a sample of runs with fiducial parameters. We show $M_{\rm cl,6} = 0.2$ (*top*), $M_{\rm cl,6} = 1.0$ (*middle*), and $M_{\rm cl,6} = 5.0$ (*bottom*).

decays until it is increased by the next injection of energy. This is similar to the pattern seen in simulations by Li & Nakamura (2006) in which turbulence in star-forming clumps $\sim$1 pc in size is maintained by energy injection from protostellar outflows. This equilibrium is maintained partly because the star formation rate responds to the current state of the cloud, increasing as the cloud contracts and its turbulence decays, and going back down when the cloud reexpands. Figure 2 shows the depletion time, defined as the ratio of the current cloud mass to the current star formation rate, which exhibits this pattern.

As shown in Figure 3, cloud column densities also show a sawtooth pattern, oscillating up and down but remaining relatively constant over multiple expansion and contraction cycles so that the time average is roughly the observed value $N_{\rm H,22} \approx 1.5$. (The figure is somewhat deceptive, because the longest lived clouds tend to go to somewhat lower column densities, and these stand out the most when examining the figure because the shorter lived clouds all overlie one another on the left side of the plot. The numerically computed time-averaged density over all models is

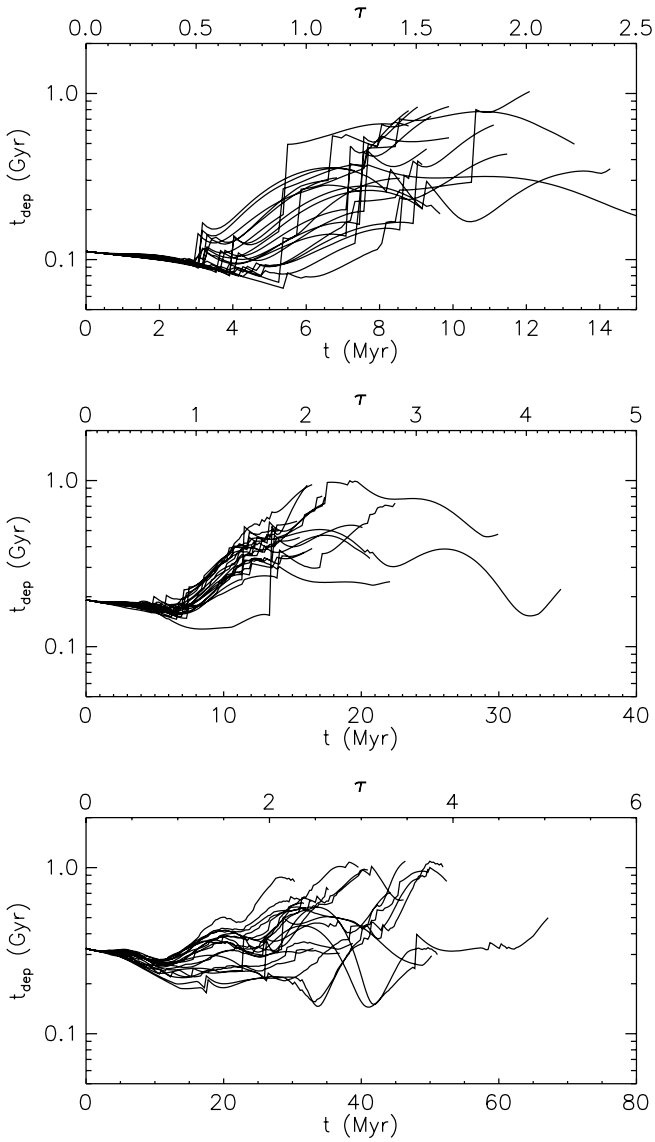

FIG. 2.—Depletion time vs. physical time t and dimensionless time τ for a sample of runs with fiducial parameters. We show $M_{\rm cl,6} = 0.2$ (*top*), $M_{\rm cl,6} = 1.0$ (*middle*), and $M_{\rm cl,6} = 5.0$ (*bottom*).

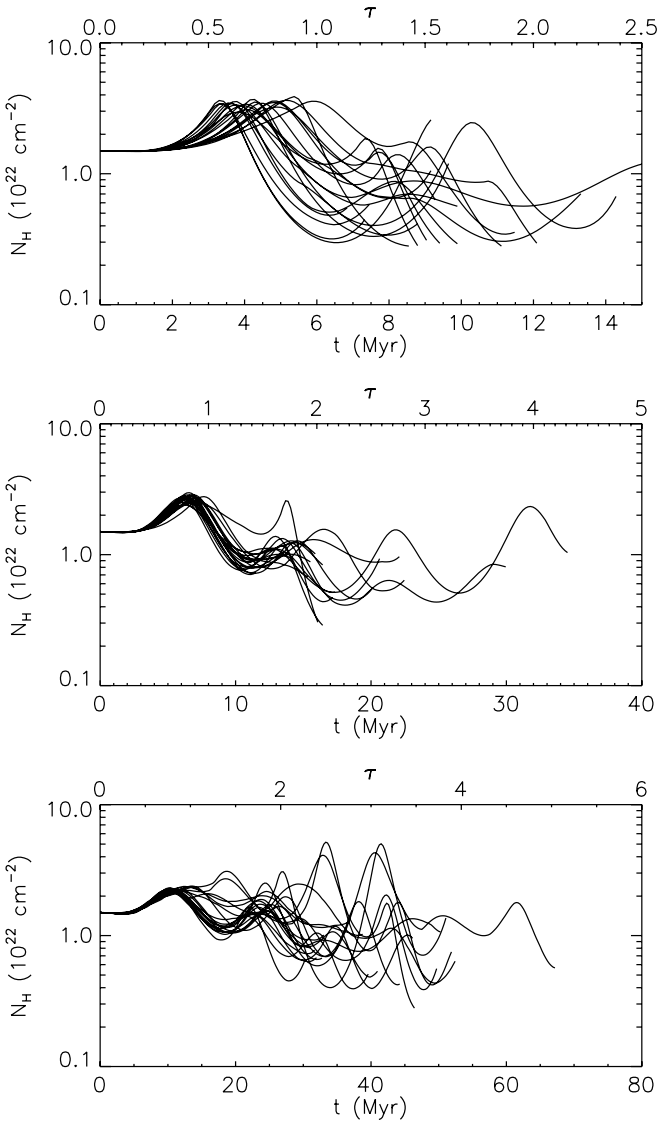

FIG. 3.—Column density $N_{\rm H}$ vs. physical time t and dimensionless time τ for a sample of runs with fiducial parameters. We show $M_{\rm cl,6} = 0.2$ (*top*), $M_{\rm cl,6} = 1.0$ (*middle*), and $M_{\rm cl,6} = 5.0$ (*bottom*).

given in Table 3.) Over their lifetimes, the average star formation efficiency of clouds, defined as the fraction of initial cloud mass transformed into stars, is 5%–10%. H II regions ionize away anywhere from 50%–90% of the mass before finally destroying the clouds entirely, with lower mass clouds losing less mass to photoionization than more massive clouds. Figure 4 shows this evolution.

The duration and stability of cloud equilibrium is affected by cloud mass. Low-mass clouds, $M_{\rm cl,6} = 0.2$ are only stable for an average of 1.6 crossing times (3.2 free-fall times), and are most often destroyed when they form an H II region that delivers enough momentum to completely unbind them. They survive only one or a few cycles of expansion and contraction. In contrast, very massive clouds, $M_{\rm cl,6} = 5$, are stable for 3.2 crossing times and for multiple cycles before finally being unbound by H II regions. At all masses most clouds are destroyed by direct disruption rather than by a photodissociation, with the number photodissociated dropping sharply as a function of mass. This result is largely a function of cloud lifetimes. Direct disruption by a single H II region occurs when a truly large association forms, one that is on the tail of the mass distribution. Since larger clouds live longer and form more stars, they sample this tail more thoroughly, and thus are more likely to form one very large association capable of disrupting them than smaller clouds. An additional effect comes from the cloud velocity dispersion. Since larger clouds have higher velocity dispersions, the H II region shells driven by small associations merge more quickly, so the relative amount of energy injected by large versus small associations increases.

Cloud disruption is much more frequent in our models than in those of Williams & McKee (1997) or of Matzner (2002). The primary difference is a revised criterion for dynamical disruption. Williams & McKee took the onset of a cometary phase to be the point at which an H II region effectively disrupts or displaces its parent cloud. Matzner considered the delivery of a momentum $p_{\rm sh}$ in excess of $M_{\rm cl} v_{\rm esc}$ to define disruption. Our criterion ($\dot{r}_{\rm sh} > v_{\rm esc}$ when $r > R_{\rm cl}$) resembles the Matzner threshold, but requires roughly half as much momentum because we model H II regions as hemispheres and clouds as spheres. In addition, our adoption of the Kroupa (2002) IMF and Parravano et al. (2003) stellar properties leads to about twice as many ionizing photons per stellar mass relative to Williams & McKee and Matzner. The revised model of

TABLE 4
OUTCOMES WITH VARYING COLUMN DENSITY

$M_{\rm cl,6}$ (1)	$N_{\rm H,22}$ (2)	$t_{\rm life}$ (3)	$\bar{\alpha}_{\rm vir}$ (4)	$\bar{N}_{\rm H,22}$ (5)	SFE (6)	$M_{\rm phot}$ (7)	$N_{\rm disrupt}$ (8)	$N_{\rm dissoc}$ (9)	$N_{\rm col}$ (10)
0.2.....	0.5	0.44 (6.1)	1.7	0.60	0.022	0.34	74	26	0
	1.5	1.6 (9.9)	2.2	1.4	0.053	0.53	63	37	0
	4.5	5.6 (15)	1.5	5.2	0.19	0.80	93	0	7
1.0.....	0.5	0.72 (15)	1.9	0.61	0.026	0.51	8	92	0
	1.5	2.2 (20)	2.1	1.3	0.054	0.70	92	8	0
	4.5	...	...	...	...	...	17	0	83
5.0.....	0.5	1.3 (41)	1.6	0.5	0.039	0.58	5	95	0
	1.5	3.2 (43)	1.5	1.5	0.082	0.80	99	1	0
	4.5	...	...	...	...	...	0	0	100

NOTES.—Col. (3): Mean lifetime in crossing times (parentheses give corresponding value in Myr). Cols. (4)–(5): $\alpha_{\rm vir}$ and $N_{\rm H,22}$ averaged over all times and runs. Col. (6): Star formation efficiency. Col. (7): Fraction of mass photoevaporated prior to cloud destruction. Cols. (8)–(10): Number of runs out of 100 that ended in disruption, dissociation, and collapse. Cases with $N_{\rm H,22} = 1.5$ are identical to the values in Table 3. We compute average quantities excluding runs that result in collapse, and we do not attempt to compute averages in cases where a majority of runs produce collapse.

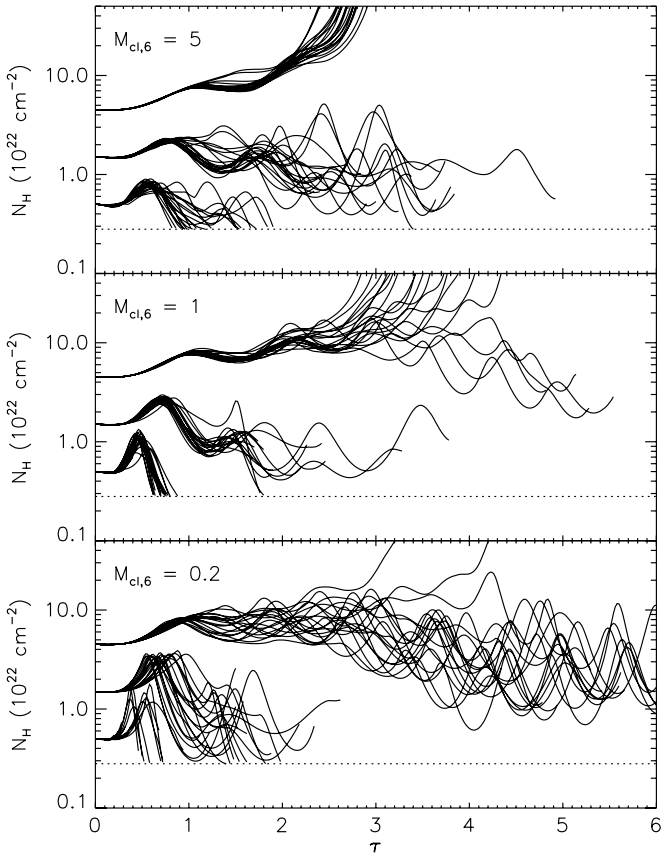

FIG. 5.—Column density $N_{\rm H}$ vs. dimensionless time τ for a sample of runs with varying initial $N_{\rm H}$. Each panel shows a different initial mass, shown in the upper left corner. The dotted horizontal line indicates the column density at which clouds dissociate.

starburst galaxy, the typical GMC column density is 2.5 times that in the Milky Way (Rosolowsky & Blitz 2005).

Table 4 gives statistical results for the runs with varying $N_{\rm H}$, and Figure 5 shows the evolution of column density versus time for a sample of runs at each mass. The results show that $N_{\rm H,22} \approx 1$ seems to be roughly a critical point in column density. Clouds that begin their evolution at substantially lower column density tend to disrupt or dissociate in $\sim$1 dynamical time. Clouds that start at higher column densities show a pattern that depends on mass. At masses $M_{\rm cl,6}$ T 1, they remain stable for long times. At higher masses, they tend to undergo uncontrolled collapse.

This change in behavior is not due to a change in the star formation rate per dynamical time. This is almost independent of the column density, since SFR$_{\rm A} \propto$ M $^{-0.32} \propto N_{\rm H}^{-0.08}$ for fixed $\alpha_{\rm vir}$. Instead, the evolution depends on the column density because column density significantly affects the efficiency of feedback. With our approximation that merged H II regions do not inject energy into clouds, the fraction of an H II region's energy that is lost to radiation increases with column density, so for equal ionizing fluxes and times, the kinetic energy in an H II region shell varies as $N_{\rm H}^{-3/5}$. Furthermore, higher column densities increase the cloud velocity dispersion (as $N_{\rm H}^{1/4}$ for fixed $\alpha_{\rm vir}$) and decrease the expansion velocity, causing H II regions to break up and merge earlier. Since in our model H II regions only gain energy as long as they are expanding, the sooner they merge the less energy they inject. From equation (35), for fixed cloud and H II region properties the ratio of the merger radius to the cloud radius scales as $N_{\rm H}^{-9/50}$. Combining these two effects, equation (38) shows that the energy injected by a single H II region of fixed properties into a cloud of fixed mass varies with column density as $N_{\rm H}^{-69/100}$. Thus, the efficiency with which ionizing photons are converted into turbulent motions is a reasonably strong function of the column density, and this picks out a particular characteristic column density at which energy injection balances loss. This turns out to be roughly the observed column density $N_{\rm H,22} \approx 1.5$. At this point we should mention one significant cautionary note: we have not explored the effects of the external environment of GMCs, and in particular the ambient pressure, on the characteristic column density. We will consider this effect in Paper II.

It is easy to understand intuitively why the critical column density above which clouds tend to collapse for masses $M_{\rm cl,6} \gtrsim 1$ should be between $N_{\rm H,22} = 1.5$ and 4.5. In the high column density case, the velocity dispersion required to hold up a cloud is almost more than H II regions can provide. H II regions cannot effectively drive turbulence to velocity dispersions larger than the ionized gas sound speed $c_{\rm II} = 9.7$ km s^{-1}, and as indicated in Table 2, in the high mass, high column density case the level of turbulence required to maintain $\alpha_{\rm vir} = 1.1$ is $\sigma_{\rm cl,0} = 9.2$ km s^{-1}. For the medium mass case it is $\sigma_{\rm cl,0} = 7.0$ km s^{-1}. Furthermore, if the cloud contracts some so that its velocity dispersion increases a bit beyond these values, then H II regions will break up and merge with the turbulence almost immediately and will therefore inject very little energy. Matzner (2002) previously discussed the inability of H II regions to maintain virial balance in systems where the required velocity dispersion exceeds $c_{\rm II}$, and our models find the same result. We discuss the implications of this in more detail in § 7.3. Note, however, that this conclusion is partially dependent on our approximation that H II regions cease driving turbulence once they cease dynamically expanding and merge, which may not be entirely correct; see § 7.4.

The long lifetime and high star formation efficiency produced at low masses and high column density also suggests an interesting interpretation: this combination of parameters may correspond to the regime of formation of individual OB associations and open clusters, which is characterized by relatively high column densities (McKee & Tan 2003) and star formation efficiencies $\gtrsim$10% (Lada & Lada 2003), and probably requires many crossing times to complete (Tan et al. 2006). Although the highest column density we have considered is still relatively modest by the standards of some cluster-forming clumps, which can reach

TABLE 5
Outcomes with Varying Dissipation Rate

$M_{\rm cl,6}$ (1)	η_v (2)	$\phi_{\rm in}$ (3)	$t_{\rm life}$ (4)	$\bar{\alpha}_{\rm vir}$ (5)	$\bar{N}_{\rm H,22}$ (6)	SFE (7)	$M_{\rm phot}$ (8)	$N_{\rm disrupt}$ (9)	$N_{\rm dissoc}$ (10)	$N_{\rm col}$ (11)
0.2.....	0.4	1.0	1.7 (10)	2.8	1.2	0.046	0.53	49	51	0
	1.2	1.0	1.6 (9.9)	2.2	1.4	0.053	0.59	63	37	0
	1.2	0.33	1.4 (8.4)	1.9	1.8	0.067	0.57	44	56	0
1.0.....	0.4	1.0	2.3 (21)	2.6	1.1	0.046	0.64	90	10	0
	1.2	1.0	2.2 (20)	2.1	1.3	0.054	0.70	92	8	0
	1.2	0.33	1.7 (16)	1.7	2.1	0.074	0.74	61	35	4
5.0.....	0.4	1.0	4.4 (60)	2.3	1.0	0.070	0.75	98	2	0
	1.2	1.0	3.2 (43)	1.5	1.5	0.082	0.80	99	1	0
	1.2	0.33	...	...	...	...	...	0	0	100

Notes.—Col. (4): Mean lifetime in crossing times (parentheses give corresponding value in Myr). Cols. (5)–(6): $\alpha_{\rm vir}$ and $N_{\rm H,22}$ averaged over all times and runs. Col. (7): Star formation efficiency. Col. (8): Fraction of mass photoevaporated prior to cloud destruction. Cols. (9)–(11): Number of runs out of 100 that ended in disruption, dissociation, and collapse. Cases with $\eta_v = 1.2$, $\phi_{\rm in} = 1.0$ are identical to the values in Table 3. As in Table 4, we compute average quantities excluding runs that result in collapse, and we do not attempt to compute averages in cases where a majority of runs produce collapse.

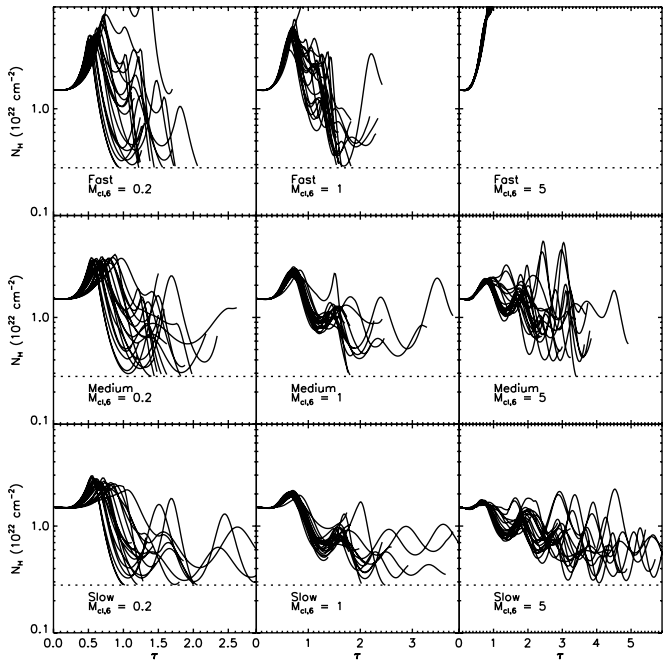

Fig. 6.—Column density $N_{\rm H}$ vs. dimensionless time τ for a sample of runs with varying dissipation rates and masses. The mass and dissipation rate are indicated in each panel. Slow is $\eta_v = 0.4$, $\phi_{\rm in} = 1.0$; medium is $\eta_v = 1.2$, $\phi_{\rm in} = 1.0$; and fast is $\eta_v = 1.2$, $\phi_{\rm in} = 0.33$. The dotted horizontal line indicates the column density at which clouds dissociate. All runs begin with $N_{\rm H,22} = 1.5$.

$N_{\rm H,22}$ of several tens, the general result that low masses and high column densities can produce long-lived bound objects is suggestive. This is particularly true in light of the recent evidence that rich clusters require $\gtrsim$5 crossing times to assemble (Tan et al. 2006; Huff & Stahler 2006; Krumholz & Tan 2006), and must therefore be held up against collapse yet not be unbound by feedback for at least this long.

6.3. *Varying Dissipation Rate*

As we discuss in § 3.1, it is possible that the turbulent dissipation rate may vary from our fiducial estimate, either being substantially lower if simulations of turbulent decay have missed some important physics, or substantially higher if the characteristic scale of molecular cloud turbulence is smaller than the size of an entire GMC. The latter possibility is probably ruled out by observations showing that turbulence in molecular clouds is self-similar out to the size of the entire GMC (e.g., Ossenkopf & Mac Low 2002; Heyer & Brunt 2004), but we explore it nonetheless to better understand how the dissipation rate affects GMC evolution. We rerun our fiducial case $\eta_v = 1.2$, $\phi_{\rm in} = 1.0$, corresponding to turbulence on the GMC scale and decay at the rate measured by Stone et al. (1998), with $\eta_v = 0.4$, $\phi_{\rm in} = 1.0$, corresponding to turbulence on the GMC scale decaying somewhat more slowly than Stone et al. find, and with $\eta_v = 1.2$, $\phi_{\rm in} = 0.33$, corresponding to turbulence driven on one-third of the GMC size scale decaying at the Stone et al. rate. Since the dissipation rate depends on the ratio $\eta_v/\phi_{\rm in}$, we are therefore considering energy dissipation rates that are a factor of 3 smaller and larger than the fiducial case. (From eqs. [15], [26], and [28], this factor of 3 larger smaller dissipation rate should correspond roughly to a factor of 3 change in the acceleration of the cloud radius, since $\mathcal{L} \propto \eta_v \sigma^3$, $\sigma' \propto \mathcal{L}/\sigma^2$, and $R'' \propto \sigma^2$.)

Table 5 summarizes the statistical results of varying the dissipation rate, and Figure 6 shows the evolution of column density versus time as a function of the dissipation rate and cloud mass. The general result is that, with the exception of the high-mass, fast-dissipation case, the results do not greatly depend on the dissipation rate. As the turbulent dissipation rate increases, the lifetime and mean virial parameter decrease and the mean column density and the star formation efficiency increase, but none of these changes by more than ~10%. That changing the dissipation rate by a factor of 3 in either direction induces a much smaller change in the cloud column density and virial parameter suggests that these values represent roughly an equilibrium configuration, and that this equilibrium is quite robust. As the dissipation rate changes by a factor of 9 from the lowest to the highest values we try, clouds contract a bit more, form stars a bit more vigorously, and are destroyed by stellar feedback a bit sooner, but only modest changes are sufficient to offset the change in dissipation rate. Star formation self-regulates to produce GMCs with $N_{\rm H,22} \approx 1$ and $\alpha_{\rm vir} \approx$ 1–2, and the regulation is stiff in the sense that even an order of magnitude change in the dissipation rate does not alter it much. We discuss reasons for this in § 7.1.

There are two exceptions to this, where varying the dissipation rate does produce a qualitative change in the outcome. For clouds of high mass and high dissipation rate, we see a phenomenon similar to the high-mass, high column density case. For $M_{\rm cl,6} = 5$, the velocity dispersion starts at $\sigma_{\rm cl,0} = 7.0$ km s^{-1}, but increases very rapidly as the cloud contracts due to decay of turbulence. By the time the first large H II regions have expanded to the point where they contain substantial kinetic energy, the cloud has contracted to the point where the velocity dispersion required to hold it up is comparable to or larger than $c_{\rm II} = 9.7$ km s^{-1}. As a result, H II regions cannot hold up the cloud, and it collapses.

The other exception occurs if we simultaneously increase the column density to $N_{\rm H,22} = 4.5$ and lower the dissipation rate by setting $\eta_v = 0.4$, $\phi_{\rm in} = 1.0$. In this case, clouds have long lifetimes and high star formation efficiencies regardless of their mass, and their column densities gradually decrease with time. Qualitatively, this is the same behavior we see for the case $M_{\rm cl,6} = 0.2$, $N_{\rm H,22} = 4.5$, and the fiducial dissipation rate. Figure 7 shows the evolution of clouds within initial column densities of $N_{\rm H,22} = 4.5$ as a function of mass and dissipation rate. As the plot shows, reducing the dissipation rate changes the characteristic mass at which one goes into the high star formation efficiency, long-lived regime. The boundary between this regime of very long stability

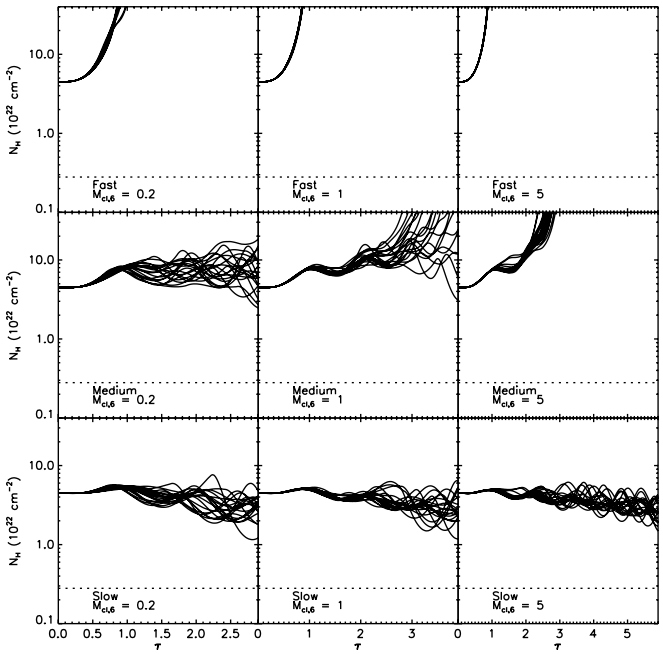

FIG. 7.—Column density $N_{\rm H}$ vs. dimensionless time τ for a sample of runs with varying dissipation rates and masses, all starting from high initial column densities. The mass and dissipation rate are indicated in each panel. Slow is $\eta_v = 0.4$, $\phi_{\rm in} = 1.0$; medium is $\eta_v = 1.2$, $\phi_{\rm in} = 1.0$; and fast is $\eta_v = 1.2$, $\phi_{\rm in} = 0.33$. The dotted horizontal line indicates the column density at which clouds dissociate. All runs begin with $N_{\rm H,22} = 4.5$.

and the regime of stability for a few dynamical times appears to depend weakly on both the mass and the dissipation rate.

6.4. *Varying Energy Injection Efficiency*

As we discuss in § 3.2.3, we are not certain of the efficiency with which H II regions are able to drive motions in turbulent media. We therefore rerun our fiducial models with $\eta_E = 0.25$, thereby reducing the amount of energy injected by H II regions by a factor of 4. This allows us to examine how strongly our results depend on our assumed efficiency.

Table 6 summarizes our results, which show how small a difference the change in driving efficiency makes. With a factor of 4 less energy injection for an H II region of the same luminosity, the mean lifetime of the lower mass clouds we model increases by about 10% and that of the highest mass clouds decreases by the same fraction. Mean virial parameters decline by ~10%, and mean

TABLE 6
OUTCOMES WITH VARYING H II DRIVING EFFICIENCY

$M_{\rm cl,6}$ (1)	η_E (2)	$t_{\rm life}$ (3)	$\bar{\alpha}_{\rm vir}$ (4)	$\bar{N}_{\rm H,22}$ (5)	SFE (6)	$M_{\rm phot}$ (7)	$N_{\rm disrupt}$ (8)	$N_{\rm dissoc}$ (9)	$N_{\rm col}$ (10)
0.2.....	0.25	1.7 (11)	1.6	1.7	0.065	0.67	93	7	0
	1.0	1.6 (9.9)	2.2	1.4	0.053	0.59	63	37	0
1.0.....	0.25	2.1 (20)	1.6	1.6	0.062	0.75	100	0	0
	1.0	2.2 (20)	2.1	1.3	0.054	0.70	92	8	0
5.0.....	0.25	2.8 (39)	1.3	1.8	0.087	0.82	100	0	0
	1.0	3.2 (43)	1.5	1.5	0.082	0.80	99	1	0

NOTES.—Col. (3): Mean lifetime in crossing times (parentheses give corresponding value in Myr). Cols. (4)–(5): $\alpha_{\rm vir}$ and $N_{\rm H,22}$ averaged over all times and runs. Col. (6): Star formation efficiency. Col. (7): Fraction of mass photoevaporated prior to cloud destruction. Cols. (8)–(10): Number of runs out of 100 that ended in disruption, dissociation, and collapse. Cases with $\eta_E = 1.0$ are identical to the values in Table 3.

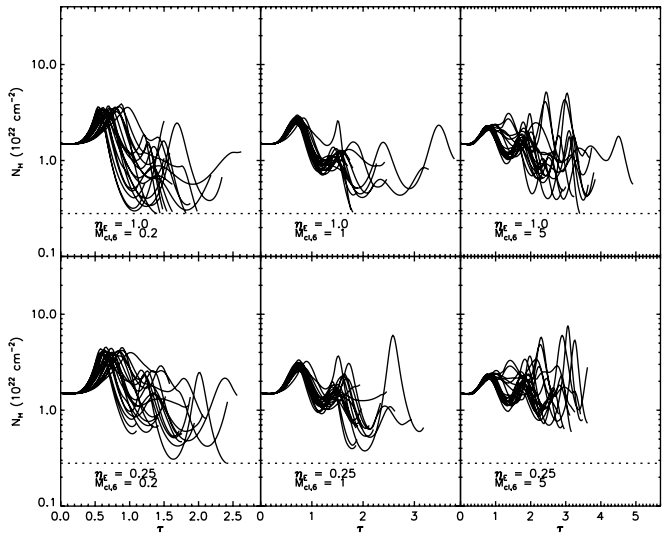

FIG. 8.—Column density $N_{\rm H}$ vs. dimensionless time τ for a sample of runs with varying H II region driving efficiencies and masses. The mass and driving efficiency are indicated in each panel. The dotted horizontal line indicates the column density at which clouds dissociate. All runs begin with $N_{\rm H,22} = 1.5$.

column densities rise a similar amount. Both star formation efficiencies and fractions of the mass photoevaporated rise, but again by only ~10%. The only quantity that changes significantly is the fraction of clouds destroyed by dissociation, which not surprisingly declines sharply. Thus, our results appear extremely insensitive to changes in the assumed energy injection efficiency of H II regions. Figure 8, which shows the evolution of column density versus time for a sample of our runs, confirms this impression. The runs with lower energy injection efficiency go to slightly higher column densities, but overall show no major difference in their evolution from the fiducial case. Again, the star formation process seems to be self-regulating, so that large changes in efficiencies, either of energy injection or of dissipation, produce only very small changes in the global statistics of cloud evolution. We discuss reasons for this in § 7.1.

7. DISCUSSION

7.1. *The Relationship of Cloud Properties to Rates of Radiative Loss and Energy Injection*

One of the most interesting results of our analysis is how little the global statistics of cloud evolution, such as lifetimes and star formation efficiencies, change in response to large changes in parameters such as the rate at which turbulence decays via isothermal shocks or the efficiency with which H II regions transfer their kinetic energy into turbulent motions. We can understand intuitively why large variations in either driving efficiency or dissipation rate cause such minimal changes in the statistics of cloud evolution by examining Figure 2. As the figure illustrates, clouds form most of their stars during their contraction phases, when they reach high densities, so the rate of star formation is effectively set by the cadence of expansion and contraction cycles. This cadence is affected only slightly by the dissipation rate and the energy injection efficiency, because both of these properties are coupled to cloud evolution poorly, with large time delays.

For a GMC to contract from an expanded state, the rate-limiting step is not the time required to dissipate the energy injected by H II regions; it is the cloud free-fall time, the time the cloud would take to collapse even if it contained no turbulence at maximum expansion. Thus, varying the turbulent dissipation rate makes little difference to the cloud contraction time. Similarly, the time it takes

for H II regions to drive apart a cloud is controlled less by the amount of energy added per unit mass of stars formed than by the time delay between when stars begin forming and when the H II regions they create expand, break up, and drive turbulent motions. Lowering the driving efficiency means that clouds expand somewhat less far, but since the dissipation rate of the turbulence is a strong function of the velocity dispersion, $\mathcal{L} \propto \sigma^3$, the extra energy at early stages produced by higher efficiency is radiated away very quickly, and produces only slightly increased cloud expansion. We can put this argument more formally by noting that our energy equation gives $\sigma' \propto \sigma^2$, neglecting changes in velocity dispersion due to external pressure and cloud expansion, so the time required for a velocity dispersion of σ_0 immediately after a large H II region breaks up to decay to a value σ_1 obeys $t \propto (\sigma_0 - \sigma_1)/(\sigma_0\sigma_1)$. If the final velocity dispersion is much smaller than the initial one, i.e., $\sigma_1 \ll \sigma_0$, this ratio is independent of σ_0. Thus, the decay time for a large amount of initial energy injected is only slightly larger than the decay time for a significantly smaller energy injection, so the cloud expansion time and maximum radius depend only weakly on the driving efficiency.

This insensitivity to the dissipation rate and the energy injection rate breaks down if the dissipation rate becomes so high or the energy injection so inefficient that H II regions are not capable of expanding clouds at all. In this case, clouds undergo runaway collapse. It also breaks down if the dissipation rate becomes so low or the efficiency so high that the first generation of H II regions simply unbinds most clouds, in which case clouds form only one generation of stars and are destroyed on a timescale set by the expansion time for H II regions from that first generation. However, in between these two extremes there is a broad range of parameter space within which the cadence of expansion and contraction cycles is set mostly by the cloud free-fall time and the time required for H II regions to break up, with only a very weak dependence on the details of the energy loss rate or the energy gain efficiency. The degree of insensitivity is illustrated by Figures 6 and 8, in which factor-of-several variations in dissipation rate or driving efficiency change the expansion and contraction period by only tens of percent.

7.2. *GMC Stability and Lifetime*

Observations place strong constraints on the stability of GMCs, and are now beginning to constrain their lifetimes as well. We must test theories that seek to explain the behavior of GMCs against these observations. The first constraint is that GMCs cannot be in a state of global collapse. If they were, then they would convert order unity of their mass into stars in a crossing time, and this would produce a star formation rate 2 orders of magnitude larger than the observed one (Zuckerman & Evans 1974). Thus, a model of GMC evolution must explain why GMCs are stable against global collapse and convert only a few percent of their mass into stars per crossing time.

The second observational constraint is that GMCs, at least the most massive ones, live for considerably more than a single crossing time. While GMC lifetimes are quite difficult to estimate inside the Milky Way, age spreads of the largest OB associations are $\sim$20 Myr (Blaauw 1964; Blitz & Shu 1980), which is a probable lower limit on the lifetimes of GMCs. More robust constraints are available in extragalactic observations, where there is no distance ambiguity. Associations between GMCs and star clusters imply a typical GMC lifetime of $\sim$20 Myr in M33 (Engargiola et al. 2003) and 27 Myr in the LMC (Fukui et al. 1999; Blitz et al. 2006). This is significantly greater than the GMC crossing time of $\lesssim$10 Myr. While the difference between 1 and a few crossing times might seem insignificant, recall that the *e*-folding time for the decay of turbulence is roughly a crossing time. A cloud 2 crossing times old will have lost almost all of its turbulence if feedback or some other source cannot replenish it, and will therefore undergo global collapse. Thus, the observations not only require that clouds be stable against collapse; they require that this stability be maintained for several turbulent decay times.

The GMC model we present in this paper, using the fiducial parameters suggested by observation and previous theoretical work, provides very good qualitative agreement with the observations. We show that feedback from star formation can keep clouds supersonically turbulent and virialized for $\sim$30 Myr, until they are destroyed by feedback. Combined with the results of Krumholz & McKee (2005) showing that supersonic turbulent motions naturally produce a star formation rate of a few percent per crossing time if star formation occurs in virialized clouds, this model satisfies both observational constraints. We discuss the question of how GMCs evolve during this lifetime in more detail in § 7.3.

Alternative models run into difficulty with one of these two observations, or with other data. One possible explanation why GMCs do not undergo global collapse is that they are gravitationally unbound transient fluctuations in the atomic ISM; only local subregions constituting a small fraction of the cloud mass are bound and can collapse (Mac Low & Klessen 2004; Clark & Bonnell 2004; Clark et al. 2005; Vazquez-Semadeni et al. 2006; Dobbs et al. 2006). However, in this case it is hard to see how GMCs could survive 20–30 Myr. For example, Clark et al. (2005) find GMC lifetimes of only about 10 Myr in their simulations of unbound clouds. There are also other severe observational difficulties. There are no molecular clouds with masses $\gtrsim 10^4\ M_\odot$ that are clearly gravitationally unbound, with virial parameters $\alpha_{\rm vir} \gg 1$, either in the Milky Way (Heyer & Brunt 2004) or in other galaxies (Engargiola et al. 2003; Rosolowsky et al. 2003; Rosolowsky & Blitz 2005; Blitz et al. 2006). There are many examples in the Milky Way of clouds of mass $< 10^4\ M_\odot$ with virial parameters $\alpha_{\rm vir} \gg 1$ (Heyer & Brunt 2004), and there is no obvious reason why massive clouds should not also display a range of $\alpha_{\rm vir}$ if they are generally unbound. Transient fluctuation models also have problems explaining the existence of a GMC mass scale and the low rotation rates of GMCs. These arguments are presented in detail in Krumholz & McKee (2005).

A second possibility is that GMCs are bound, at least marginally, but that they are destroyed before the turbulence with which they are born decays away. As a result, they never have a chance to begin global collapse. However, the observed lifetimes of $\gtrsim$20 Myr appear to rule out the possibility that such rapid destruction is the norm. Furthermore, to work this model requires a mechanism of cloud destruction that reliably operates in $\lesssim$1 crossing time. As we show here, H II regions are not capable of completely photoevaporating or disrupting massive clouds over such short periods. Supernovae and protostellar winds inject considerably less energy into GMCs per unit mass of stars formed than do H II regions (Tenorio-Tagle et al. 1985; Yorke et al. 1989; Matzner 2002), so they are unlikely candidates for rapid cloud disruption. In the absence of a plausible mechanism for cloud disruption in $\sim$10 Myr, this model faces a major theoretical problem as well as an observational one.

It is worth noting at this point that arguments for GMC lifetimes in the Milky Way strictly limited to 1 crossing time, e.g., Hartmann et al. (2001), generally rely on observations of clouds in the solar neighborhood, all of which are much smaller than the larger, more typical GMCs we have considered in this paper. Since we find that molecular clouds $\lesssim 10^5\ M_\odot$ in mass do only survive for $\sim$1 crossing time, our results are consistent with the idea that solar neighborhood GMCs are short-lived. We simply suggest that

GMC lifetime is mass-dependent and that the nearest clouds, due to their atypical masses, also have atypical lifetimes.

7.3. *An Evolutionary Scenario for GMCs*

Our findings allow us to present a rough evolutionary scenario for GMCs that is consistent both with the constraints of stability and GMC age described in § 7.2 and with the observation that GMCs in the Milky Way and in other galaxies all lie in a narrow range of column densities and virial parameters, centering around $N_{\rm H,22} \approx 1.5$ and $\alpha_{\rm vir} \approx 1$–2. (Larson 1981; Solomon et al. 1987; Blitz et al. 2006). This scenario is quite similar to that suggested in McKee (1989) and is developed in considerably greater detail in Paper II.

Our scenario is that GMCs are born at low column densities by condensation out of the atomic ISM, primarily triggered by self-gravitational instabilities in spiral shocks (e.g., Kim & Ostriker 2001; Kim et al. 2002, 2003). This can only occur in regions of a galactic disk that are at significantly higher densities and pressures than is typical of the ISM. If star formation were able to start in such clouds immediately, they would undergo rapid disruption, converting $\lesssim$3% of their mass into stars. However, in reality such clouds are probably not star-forming over most of their volume, so feedback is suppressed.

This may explain the observation that GMCs pass through a phase in which they appear to lack embedded H II regions. The duration of this phase is difficult to obtain from observations; Fukui et al. (1999), Engargiola et al. (2003), and Blitz et al. (2006) report that $\sim\frac{1}{4}$ of GMCs do not show Hα signatures associated with H II regions, but this is probably an overestimate because it does not include highly obscured H II regions. Although the Hα sensitivities of the catalogs used by these authors are sufficient to detect H II regions with Hα luminosities comparable to the Orion Nebula, Orion is visible largely because it is on the near side of a dark cloud; at the distance of the LMC or M33, Orion would be invisible if it were oriented with the dark cloud on the near side rather than the other way around. *Spitzer* MIPS observations have failed to find any GMCs that are dark at 24 μm, so there must be some embedded star formation even in GMCs without detected H II regions (E. Rosolowsky 2006, private communication). This result suggests either that the H II regions surveys are incomplete, or that clouds do not begin making massive stars until well after they have begun forming low-mass stars, an effect we have not considered.

Regardless of how long this initial starless phase lasts, a question we will address using our models in Paper II, in the absence of feedback, GMCs will contract due to loss of turbulent support, gravity, and external pressure, until they approach $N_{\rm H,22} \approx 1$. At that point, they become star-forming, and feedback stabilizes them against further contraction and keeps them in virial equilibrium for several crossing times. We observe GMCs at $N_{\rm H,22} \approx 1$, $\alpha_{\rm vir} \approx 1$–2 because this is where they spend the vast majority of their lifetimes. This column density is selected because it is the one for which energy injection by turbulence roughly balances energy loss by isothermal shocks. In addition to turbulent energy injection, the recoil momentum produced by mass being evaporated by H II regions may also play a significant role in confining clouds.

This quasi-equilibrium endures for an amount of time that depends on the cloud mass. For massive clouds, which contain most of the molecular mass in the Milky Way and in all but one other galaxy in which it is possible to estimate cloud mass distributions (Fukui et al. 1999; Engargiola et al. 2003; Blitz et al. 2006), it endures 2–3 crossing times, or 20–30 Myr. During a cloud's lifetime, it converts 5%–10% of its mass into stars. These results are robust against changes in the assumed dissipation rate for turbulence or efficiency of turbulent driving by H II regions. Less massive clouds are probably dynamically disrupted in $\sim$1 crossing time, consistent with estimates of the lifetimes of small clouds in the solar neighborhood (e.g., Hartmann et al. 2001), although parts of them may endure in molecular phase and continue forming stars for longer periods of time even after the original cloud has been disrupted.

One interesting question is how our results might change if we considered a galaxy quite different from the Milky Way. Observations indicate that GMCs in normal spiral galaxies like the Milky Way are generally quite similar to those in the Milky Way (Blitz et al. 2006), so to find truly different conditions we must consider galaxies that are approaching the regime of starbursts. The sole observational example of such a galaxy where we have observed the clouds is M64, a weak starburst in which the largest GMCs are $\gtrsim 10^7\ M_\odot$ in mass, and have surface densities up to $N_{\rm H} \approx 4 \times 10^{22}$ cm^{-2} (Rosolowsky & Blitz 2005). Despite these differences from Milky Way GMCs, observations indicate that these clouds are still in approximate virial balance, and that like Milky Way GMCs their star formation rate is only a few percent per free-fall time. Thus, they are not in a state of global collapse.

Since we have found that H II regions cannot sustain the turbulence and prevent collapse in such clouds (although see § 7.4), we are left with two possibilities. Either the dissipation rate in such clouds is lower than our fiducial estimate, or there is an additional source of energy input that supplements H II regions. One strong candidate for a source of energy injection is driving of turbulence by external shocks (Kornreich & Scalo 2000), either from supernovae, gravitational instabilities driven by the potential of the stars, or cloud-cloud collisions (Tan 2000). This mechanism encounters considerably difficulty in the Milky Way because GMCs are much denser than the gas around them in which shocks propagate. This creates an "impedance mismatch" that makes it difficult to drive turbulence into the GMCs (Nakamura et al. 2006). However, in a starburst where the ISM is entirely molecular, clouds are not much denser than their surroundings. Rosolowsky & Blitz (2005) find that in M64 the GMCs are overdense only by factors $\sim$2. This removes the impedance mismatch problem, and makes it far easier for external shocks to drive turbulence than it is in galaxies like Milky Way. Whether this mechanism can work in detail will require more analytic models and simulations to determine.

7.4. *Limitations of This Model*

The most obvious limitation of our model is the constraint that GMCs evolve homologously. In mathematical terms, this constraint is equivalent to dropping time derivatives of a_I in the virial theorem. This should only change our results substantially if changes in the moment of inertia of a GMC occurred primarily through changes in its shape rather than overall expansion or contraction. While a cloud in approximate equilibrium probably does experience most changes in its inertia via changes in shape, a cloud that is undergoing global collapse or global disruption would almost certainly experience most changes in its inertia through those processes rather than through changes in shape. As a result, our broad conclusion that neither overall collapse or disruption occur for several crossing times seems likely to be robust.

A more subtle limitation to our model is our simple boundary conditions for GMCs. For simplicity we have assumed a fixed mass budget and a fixed external pressure that puts GMCs into pressure balance initially. In reality, GMCs may start forming stars while still accumulating gas. The somewhat higher mean mass for GMCs with associated H II regions than for GMCs without such associations seen in the LMC (Fukui et al. 1999; Blitz et al. 2006) seems to point in this direction. In addition, GMCs